Measurement System of the Mean and Sub-Cycle LV Grid Access Impedance From 20 kHz To 10 MHz

Igor Fernández ⬮, *Member, IEEE*, Alexander Gallarreta ⬮, *Graduate Student Member, IEEE*, Jon González-Ramos ⬮, *Graduate Student Member, IEEE*, Paul Wright ⬮, David de la Vega ⬮, *Senior Member, IEEE*, Itziar Angulo ⬮, *Member, IEEE*, and Amaia Arrinda ⬮, *Senior Member, IEEE*

Abstract—This work presents a novel measurement method to characterize long-term and short-term variations of the LV grid impedance from 20 kHz to 10 MHz with configurable time, frequency and amplitude resolutions. The characterization of the grid access impedance in this frequency range is vital for the design and development of NB-PLC and BB-PLC technologies. The measurement system is valid for in-home, indoor cable networks and for the harsh conditions of the LV distribution grid, where a large input dynamic range and strong protection mechanisms against high-amplitude impulsive noises are required. Its accuracy is evaluated by comparison to a precision impedance meter for a wide set of impedance values, obtaining a maximum deviation within ±8%. First trials of the grid impedance sub-cycle variations caused by commercial appliances and for frequencies assigned to BB-PLC are also presented in this paper. The results demonstrate that the grid impedance is highly time-varying within the mains cycle, both in amplitude and phase. These first outcomes point at the need to evaluate the accumulative effects of sub-cycle variations in the LV distribution grid, so that equalization algorithms in the next BB-PLC technologies could be developed to overcome the impact of these fast variations.

Index Terms—Communication channels, impedance measurement, low voltage, measurement techniques, power distribution networks, power line communications.

I. INTRODUCTION

NARROWBAND Power Line Communications (NB-PLC) at frequencies up to 500 kHz are currently one of the preferred options for smart metering purposes in the Low Voltage (LV) grid. They rely on the electrical grid as the propagation medium for data transmission, taking advantage of the wired infrastructure already deployed to the end-users [1], [2], [3],

[4], [5], [6], [7], [8], [9], [10]. Recently, new data transmission technologies for the LV grid are being considered in frequencies above 1 MHz (Broadband Power Line Communications or BB-PLC) to avoid high-level disturbances and to use broader bandwidth. Although some of these technologies are already in use for home area networks and high-speed internet applications [1], [2], [4], the performance of the LV distribution grid for the propagation of these signals above 1 MHz is yet to be characterized.

The access impedance of the LV electrical grid is one of the major factors affecting PLC, as it conditions the propagation distance of the signals [8], [11], [12], [13]. It is also a key factor when designing communication devices connected to the grid [14], as the injected voltage of the transmitted signals depends on the impedance mismatching between the transmission device and the grid access impedance. The impedance mismatch results in signal reflection, which degrades the signal power transfer, and affects the communication reliability [4], [11], [15], [16], [17], [18].

Another relevant aspect is the sub-cycle grid impedance variations. Electronic equipment based on switched components (such as power supplies, AC/DC converters, and inverters) presents time-variant behavior of the impedance within the mains cycle [18], [19], [20], [21], [22], [23]. Moreover, these sub-cycle variations are highly frequency dependent, especially when frequencies above 500 kHz are considered. The characterization of the sub-cycle impedance variations in the LV distribution grid is an important part for developing and deploying PLC technologies since it is directly related to the performance of channel estimation and equalization.

Distribution grid impedance has been widely analyzed in literature for frequencies related to the fundamental harmonics and covering low frequencies up to a few kHz, as it is related to power quality and oscillatory stability analysis by applying impedance-based stability criteria [24], [25], [26], [27], [28], [29], [30]. For on-field measurements, some authors have considered non-invasive measurement methods to determine the grid impedance, which are methods that rely on naturally occurring grid events that generate harmonics as a grid excitation [26], [27]. These methods are easier to implement (only voltage and current measurements are required), but they are limited to frequencies below 2 kHz.

For frequencies above 2 kHz, invasive measurement methods must be applied. Under laboratory conditions, commercial

Impedance Analyzers and Network Analyzers are usually used. However, this type of commercial equipment is not valid for field measurements, as the coupling devices and the protection circuits that must be included to protect the system may have a significant effect on the measurement accuracy [11], [15], [24], [25], [29], [30].

A comparison of three LV grid access impedance measurement systems has been recently published in [31] for frequencies up to 500 kHz, including a measurement system developed by the authors. Another access impedance measurement system is presented in [11]. However, due to hardware limitations, none of these systems can be directly adapted to frequencies in the range of MHz.

Regarding sub-cycle variations, some previous works present measurements of the impedance behavior within the fundamental cycle. Nevertheless, they are limited to frequencies up to 500 kHz [11], [32], [33] or 1 MHz [34], or analyze indoor power line channels [18], [23], [35].

In this context, as far as the authors are aware, there is no LV grid access impedance measurement system adapted to operate in the challenging conditions of the LV distribution grid, covering the frequencies assigned for NB-PLC and BB-PLC, and configurable to obtain the mean grid access impedance (long-term variations) or the sub-cycle grid access impedance (short-term variations).

This paper covers that gap presenting a measurement system for laboratory and on-field characterization of the access impedance of the LV electrical grid from 20 kHz up to 10 MHz. The system provides detailed results about the grid access impedance as a function of frequency and time. Depending on the selected configuration, the mean grid access impedance or the sub-cycle grid access impedance is provided.

The paper describes the measurement setup and the signal processing to obtain the long-term and short-term variations of the access impedance of the grid, along with an in-depth accuracy assessment. Then, some results of laboratory measurements of sub-cycle impedance variations are shown and analyzed.

II. MEASUREMENT SYSTEM FOR LV GRID ACCESS IMPEDANCE ASSESSMENT UP TO 10 MHZ

The measurement system presented in this paper is an upgraded version of the system described in [31], with extended frequency range up to 10 MHz and analysis of sub-cycle variations.

A. Basis of the Measurement Procedure

The method is based on the measurement of both voltage and current generated by a test signal injected into the grid. The access impedance of the grid corresponds to the voltage to current ratio for each frequency component (n) within the frequency range under test (20 kHz to 10 MHz).

Accordingly, the measurement system generates and injects a test signal into the grid, and then, it acquires and stores accurate recordings of voltage and current waveforms synchronously. The post-processing assessment of the registered data, based on Fourier analysis and developed in Matlab, provides the spectral
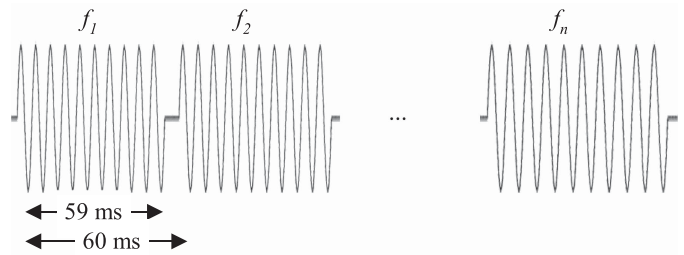

Fig. 1.   Test signals to measure frequency-dependent grid impedance.

characterization of the complex values of voltage, current, and grid impedance (amplitude and phase, or real and imaginary parts) [31], [36].

B. Test Signal

In order to be able to analyse the sub-cycle impedance variations, the configuration of the test signal used in the previous system proposed by the authors is no longer valid [31], as now we need to measure at least one cycle per frequency. For the measurement system described here, the test signal is composed of a set of short single-frequency bursts, transmitted sequentially at specific discrete frequencies, which cover the range under study (20 kHz to 10 MHz).

The frequency resolution is determined by the separation between adjacent discrete frequencies selected for the measurement. Depending on the frequency band to be considered, the number and duration of the single-frequency bursts define the frequency resolution and the time required to cover the whole frequency range. Hence, a higher number of bursts implies a better resolution in the frequency domain but a longer measurement time; on the contrary, faster measurements can be done with a lower number of discrete frequencies. A trade-off configuration between the frequency resolution (the number of the discrete frequencies that are measured) and the time needed to cover the whole frequency band must be applied. It should be noted that the system assumes quasi-stationary impedance conditions, i.e., that the grid conditions do not change during the measurement time. This means that the impedance values obtained for each frequency burst correspond to the same situation, obtaining the time variability of the impedance within the fundamental cycle for the whole frequency band of interest.

In the following paragraphs, as an example, the selection of the required parameters for measuring the frequency band from 250 kHz to 10 MHz is explained.

Duration of the bursts: The duration of each burst should cover, at least, a complete cycle of the mains (20 ms for 50 Hz), to which a guard interval of several ms should be added in order to account for possible time deviations of the signal generator and other hardware limitations. Then, a gap between single-frequency bursts is also needed due to the specifications of the signal generator. For the specific hardware used in this study, a tentative configuration consists of injecting single-frequency bursts of 59 ms length, with a 1 ms gap between consecutive bursts (see Fig. 1).
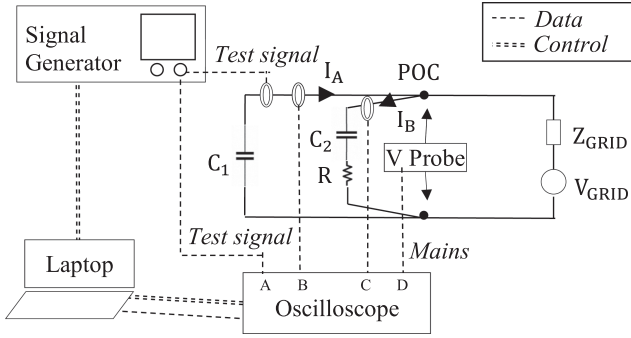
Fig. 2. Measurement setup for characterizing the sub-cycle variations of the electrical grid impedance.

Total measurement time: as the system assumes quasi-stationary impedance conditions, the total measurement time should be limited as much as possible. It was decided to limit the total measurement time to 3 s for the whole frequency range. Due to limitations of the sampling frequency of the oscilloscope when measuring from 250 kHz to 10 MHz, measurement data were limited to 1 s per file.

Frequency resolution: The selection of the frequencies of the bursts depends on the frequency band under study, the frequency resolution needed, and potential hardware limitations. Considering the limitation of 1 s per file and the duration of 59+1 ms commented above, there would be 16 bursts per file. Since there were problems with the first burst generated, we limited this amount to 14 bursts per file, so that a maximum of 42 bursts would be included in the total measurement time of 3 s. From 250 kHz to 10 MHz, this would lead to a frequency resolution of 232 kHz, so it was decided to set the frequency resolution to 250 kHz.

Therefore, an example configuration could be formed by a set of bursts from 250 kHz to 10 MHz with 250 kHz frequency steps, each lasting 59 ms and including a 1 ms gap between them, thus requiring 3 s of measurement to cover the whole frequency range.

C. Measurement Setup

The schematic of the measurement system is shown in Fig. 2. The signal generator produces the test signal that is injected into the grid, which allows calculating the access impedance of the grid as the voltage to current ratio generated by the test signal at the point of connection (POC). Additional circuitry is used for high-pass filtering of the test signal injection (shunt capacitor in Fig. 2, nominal value $C_1 = 560$ nF). The high-pass filter is adjusted to remove the fundamental component, low-order harmonics, and potential emissions below 2 kHz, considerably increasing the amplitude resolution of the system for the frequency band of interest.

In the earlier version of the system [31], voltage probes were used for injecting the test signal and decoupling the resulting voltage. However, this approach is no longer valid for frequency bands above 500 kHz. The frequency response of voltage probes

should be flat for the whole frequency band of interest and for a wide range of expected grid impedance values, but at high frequencies, resonances lead to erroneous measurements [17].

Now, a current coupler injects the test signal into the parallel branch that closes the loop. Furthermore, in order to calculate the voltage generated by the test signal at the POC of the grid, the current over a previously characterized branch (RC_2 in Fig. 2, nominal values R = 100 Ω and C_2 = 560 nF) is obtained with another current probe. This branch needs to be carefully designed and characterized. The characterization needs to be very accurate, as for high frequencies, nominal values are no longer applicable.

Another enhancement with respect to the previous version of the system is the possibility to analyse sub-cycle variations of the impedance. If the sub-cycle variations are to be characterized, an active voltage probe (indicated as V probe in Fig. 2) is used to obtain a reference of the mains voltage and detect the zero-crossings.

A digital oscilloscope acquires and samples the different signals at a sufficiently high sampling rate to avoid aliasing effects. The current and voltage probes outputs are connected to separate oscilloscope channels for synchronous recording. The test signal is also sent to the oscilloscope and recorded by the measurement system for synchronization purposes in post-processing tasks. As illustrated in Fig. 2, channel A is used for the generated test signal, channel B for the injected test current $\overrightarrow{I_A}$, channel C for the current through the parallel branch $\overrightarrow{I_B}$, and channel D for the mains voltage.

A laptop is in charge of configuring the test signals, automating the measurements, and storing the recordings for post-processing.

D. Signal Processing

A discrete-time STFT (Short Time Fourier Transform) is applied to the sampled recordings of the grid currents generated by each burst of the test signal. The calculation is developed, firstly, by a sliding time windowing based on a Gaussian 1/3 ms window, with 75% overlapping. This configuration of the time windowing provides a time resolution of 83.33 μs; nevertheless, the configuration can be modified for reducing the processing burden.

Secondly, a Fast Fourier Transform is applied to each output of the time windowing, to obtain the frequency components of the grid currents generated by the test signal: $\overrightarrow{I_A}(f_n)$ and $\overrightarrow{I_B}(f_n)$, where n is the index of the frequency component. As a result, the spectrum of the currents is obtained every 83.33 μs (considering the previous configuration). The access impedance of the grid at the POC $\overrightarrow{Z}_{POC}(f_n)$ is calculated as the voltage to current ratio generated by the test signal for each frequency component, which can be formulated as:

$$\overrightarrow{Z}_{POC}(f_n) = \frac{\overrightarrow{V}_{POC}(f_n)}{\overrightarrow{I}_{POC}(f_n)} = \frac{\overrightarrow{Z}_{RC_2}(f_n) \cdot \overrightarrow{I_B}(f_n)}{\overrightarrow{I_A}(f_n) - \overrightarrow{I_B}(f_n)} \quad (1)$$

Hence, the magnitude and phase of the grid impedance are calculated from the complex values of $\overrightarrow{Z}_{POC}(f_n)$ as

$$\left|\overrightarrow{Z}_{POC}(f_n)\right| = \sqrt{\mathrm{Re}\left\{\overrightarrow{Z}_{POC}(f_n)\right\}^2 + \mathrm{Im}\left\{\overrightarrow{Z}_{POC}(f_n)\right\}^2}$$

$$\angle\overrightarrow{Z}_{POC}(f_n) = \arctan\left\{\frac{\mathrm{Im}\left\{\overrightarrow{Z}_{POC}(f_n)\right\}}{\mathrm{Re}\left\{\overrightarrow{Z}_{POC}(f_n)\right\}}\right\}$$

(2)

where $\mathrm{Re}\{\overrightarrow{Z}_{POC}(f_n)\}$ and $\mathrm{Im}\{\overrightarrow{Z}_{POC}(f_n)\}$ represent the real and imaginary parts of the complex values of $\overrightarrow{Z}_{POC}(f_n)$, respectively.

With this method, the impedance is calculated iteratively for every burst that composes the test signal. It might be the case that some power electronic devices introduce non-intentional emissions in the frequency band of interest, which may overlap with the current injected by the measurement system. In order to avoid this, if the level of the signal injected by the measurement system is not several orders of magnitude above the non-intentional signal, that single frequency is discarded and the impedance value corresponding to that frequency burst is obtained by interpolation from adjacent values.

As the bursts are single-frequency waveforms, the number of the discrete frequencies in the bursts of the test signal determines the frequency resolution of the outcome. Additionally, the time resolution is determined by the overlap level of the time windowing in the data processing. In summary, the frequency resolution is determined by the configuration of the test signal, and a higher resolution requires longer test signals and measurement times; in contrast, the time resolution depends on the signal processing, which is linked to the computational burden.

III. ACCURACY ASSESSMENT

A. Approach and Methodology

The IEC 61557-3 standard [37], which specifies the requirements for loop impedance measuring and monitoring equipment in LV distribution systems, determines a maximum measurement uncertainty of $\pm 30\%$, considering the measured value as a reference. This tolerance limit is also determined in standards about testing and measurement techniques such as IEC 61000-4-19:2014, which defines the test conditions for immunity in the frequency range from 2 kHz to 150 kHz [38].

In this work, the accuracy of the impedance measurement system was assessed by comparing the outputs of the measurement system with respect to the measurements of a precision Impedance Analyzer [39]. This precision meter provides high accuracy over wide impedance range and frequencies up to 10 MHz for component, semiconductor and materials measurement in controlled laboratory conditions. Specifications of the maximum deviation of the precision meter are given in Table I [39].

As commented in Section I, these commercial products are not valid for measurements in the LV grid. Therefore, this meter was used as a reference meter for a set of precision resistor samples of a wide range of values, measured off-line. The nominal values and tolerances of the set of precision resistors used in the assessment were the following: 0.5 Ω (1%), 2 Ω (1%), 5 Ω (1%),

TABLE I
MAXIMUM DEVIATION SPECIFICATIONS OF THE PRECISION IMPEDANCE
ANALYZER [39]

Frequency range	Maximum deviation
9 kHz – 1 MHz	± 0.5 % for impedance values between 0.5 and 10 Ω
	± 0.1 % for impedance values between 10 and 50 Ω
	± 0.08 % for impedance values greater than 50 Ω
1 MHz – 5 MHz	± 0.5 % for impedance values greater than 5 Ω
5 MHz – 10 MHz	± 1.0 % for impedance values greater than 2 Ω
Other cases	From ± 0.5 % to ± 5.0 %, depending on the frequency and impedance value

(a)

(b)
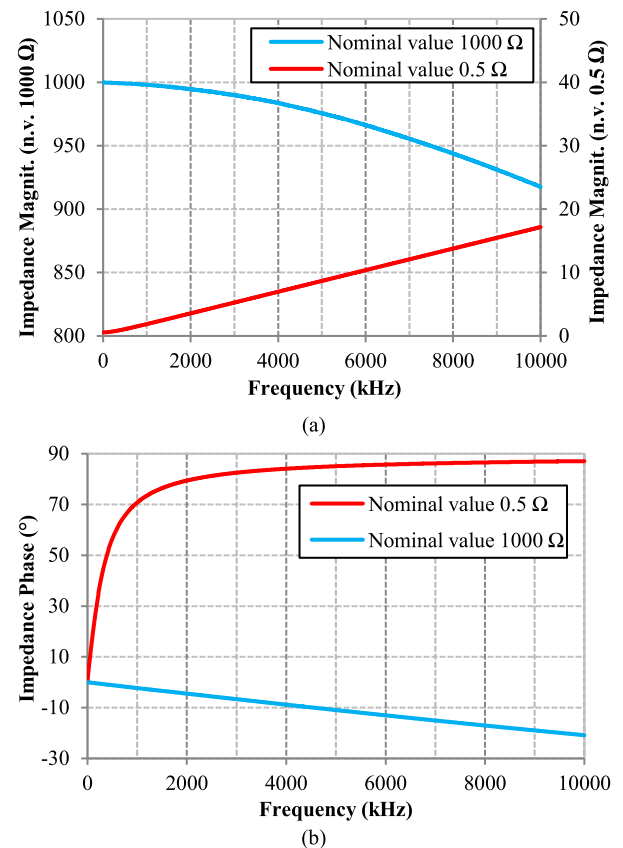
Fig. 3. Impedance magnitude (a) and phase (b) of two precision resistors with nominal values (n.v.) 0.5 Ω and 1000 Ω, measured by the precision Impedance Analyzer.

10 Ω (0.25%), 34 Ω (0.1%), 50 Ω (0.1%), 100 Ω (0.1%), 200 Ω (0.1%), 750 Ω (0.1%), 1000 Ω (1%). These resistance values cover the wide range of impedances expected to be found in the LV grid for frequencies up to 10 MHz. It must be noted that the nominal values of the resistors are only for low frequencies; for high frequencies, inductive and capacitive effects become relevant, and therefore, the test set covered a wide range of complex impedance values. This aspect is shown in Fig. 3 for two of the resistors (nominal values 0.5 Ω and 1000 Ω, lowest and highest values from the set of precision resistors).

For each resistor, 10 measurement rounds were developed with the proposed measurement system, in order to evaluate the accuracy and the stability of the obtained results. The frequency range evaluated in the trials is 20 kHz–10 MHz, with

a frequency resolution of 10 kHz (999 measurement points for each frequency sweep).

B. Results

The differences between the outputs of 10 measurement rounds with the proposed measurement system $\left(\overrightarrow{Z}_i(f_n) \text{ for } i = \{1, \dots, 10\}\right)$ and a single output with the reference Impedance Analyzer $\left(\overrightarrow{Z}_{ref}(f_n)\right)$ were calculated for each frequency bin f_n as follows:

$$
\begin{aligned}
&Diff\_Zmag_i\,(f_n) \\
&= \frac{\left|\overrightarrow{Z}_i(f_n)\right| - \left|\overrightarrow{Z}_{ref}(f_n)\right|}{\left|\overrightarrow{Z}_{ref}(f_n)\right|} \cdot 100 \quad \text{for } i = \{1, \dots, 10\} \quad (3) \\
&Diff\_Zphase_i\,(f_n) \\
&= \angle \overrightarrow{Z}_i\,(f_n) - \angle \overrightarrow{Z}_{ref}\,(f_n)
\end{aligned}
$$

With the data set corresponding to each frequency bin f_n ordered from smallest to greatest, the median value and the standard deviation of the differences were obtained as follows:

$$
\begin{aligned}
&MedianDiff\_Zmag\,(f_n) \\
&= \frac{Diff\_Zmag_5\,(f_n) + Diff\_Zmag_6\,(f_n)}{2} \quad (4)
\end{aligned}
$$

$$
\begin{aligned}
&StdDevDiff\_Zmag\,(f_n) \\
&= \sqrt{\frac{1}{9} \sum_{i=1}^{10} \left(Diff\_Zmag_i\,(f_n) - \mu_{mag}\,(f_n)\right)^2}, \quad (5)
\end{aligned}
$$

where $\mu_{mag}\,(f_n) = \frac{1}{10} \sum_{i=1}^{10} Diff\_Zmag_i\,(f_n)$

$$
\begin{aligned}
&MedianDiff\_Zphase\,(f_n) \\
&= \frac{Diff\_Zphase_5\,(f_n) + Diff\_Zphase_6\,(f_n)}{2} \quad (6)
\end{aligned}
$$

$$
\begin{aligned}
&StdDevDiff\_Zphase\,(f_n) \\
&= \sqrt{\frac{1}{9} \sum_{i=1}^{10} \left(Diff\_Zphase_i\,(f_n) - \mu_{phase}\,(f_n)\right)^2}, \quad (7)
\end{aligned}
$$

where $\mu_{phase}\,(f_n) = \frac{1}{10} \sum_{i=1}^{10} Diff\_Zphase_i\,(f_n)$

Results for the difference in amplitude are shown in Figs. 4 and 5, and results for the impedance phase are shown in Figs. 6 and 7.

The results show that, for some resistor values, the differences are slightly greater for higher frequencies; however, the differences are not correlated to the magnitude of the impedance under test. In any case, the median of the magnitude differences is always within $\pm 8\%$, and for most of the cases within $\pm 4\%$ (see Figs. 4 and 5). The median of the phase differences is always within $\pm 4°$, as shown in Figs. 6 and 7. The standard deviations of the measurements of different rounds are low (less than 1.5% in magnitude and less than 2.5° in phase for the majority of precision resistors and frequency bins), which represents that the measurement system is steady and stable.
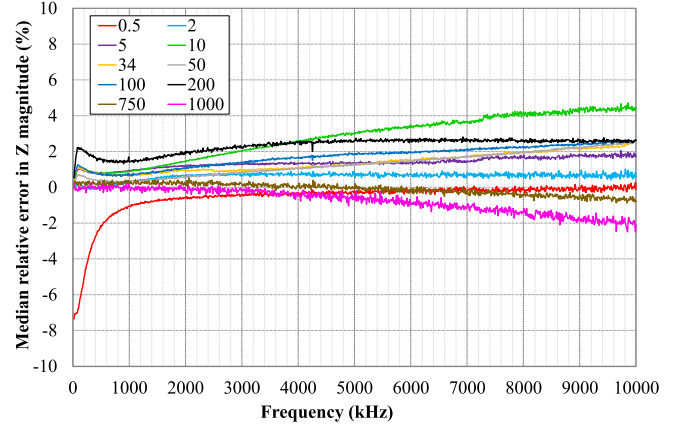

Fig. 4. Median values of the differences of the impedance magnitude (in %) for the set of precision resistors with respect to the reference meter.
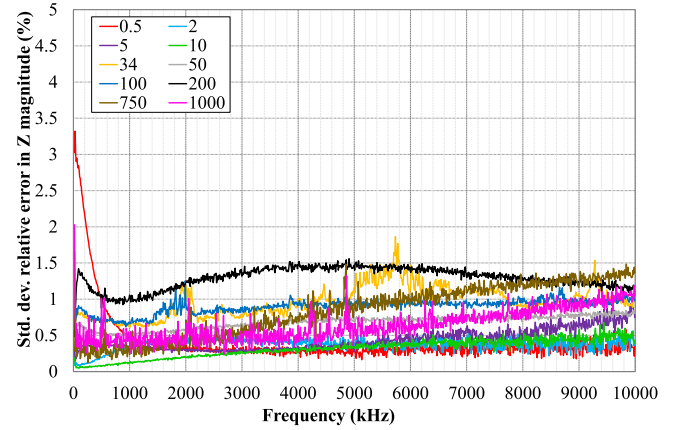

Fig. 5. Standard deviation of the differences of the impedance magnitude (in %) for the set of precision resistors with respect to the reference meter.
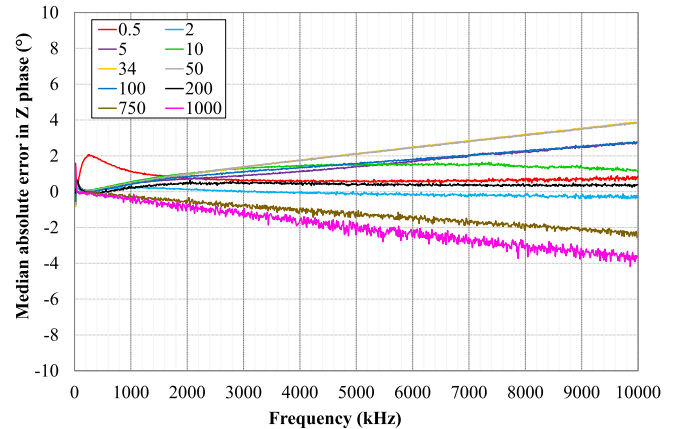

Fig. 6. Median values of the differences of the impedance phase (in degrees) for the set of precision resistors with respect to the reference meter.

The IEC 61557-3 [37] and the IEC 61000-4-19 [38] standards determine a maximum measurement uncertainty of $\pm 30\%$ for the whole frequency range and for the wide range of impedances expected to be found in the LV grid. Although the statistical evaluation type A 1 sigma uncertainty developed in this study
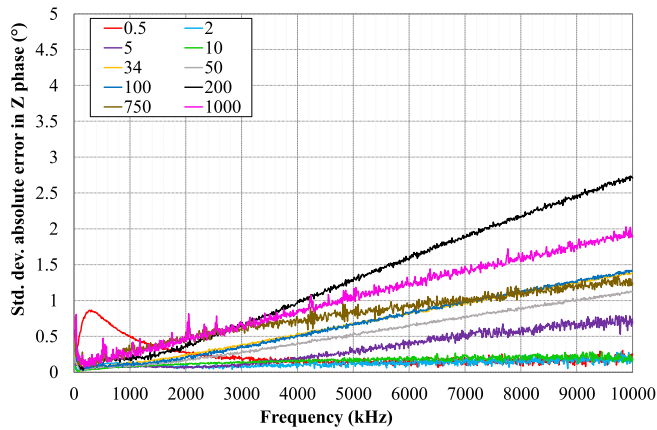
Fig. 7. Standard deviation of the differences of the impedance phase (in degrees) for the set of precision resistors with respect to the reference meter.

for accuracy assessment cannot be directly compared to this reference value, results show that obtained differences (always within $\pm$ 8%, mostly within $\pm$4%) are far from the $\pm$ 30% uncertainty determined by the standards.

Regarding the performance of the proposed method for measuring LV grid access impedances, the previous version of the system was compared to measurement systems from the Institute Systems Engineering at HES-SO Valais-Wallis and from the Institute of Electrical Power Systems and High Voltage Engineering at Technische Universitaet Dresden (TUD) in the frequency range assigned to NB-PLC (up to 500 kHz). This comparison was performed both off-line (using passive EMC filters) and on-line (field trials in a LV grid in Switzerland). The results from the three systems offered very good correlation [31]. However, a similar performance comparison for frequency ranges above 1 MHz is not possible, since, as far as the authors are aware, there is no other measurement system available.

IV. ANALYSIS OF SUB-CYCLE IMPEDANCE VARIATIONS

The potential impact of sub-cycle impedance variations generated by electronic devices in the grid access impedance has been evaluated in this work in laboratory trials. For this purpose, a set of commercial appliances containing switching-based electronics elements were selected and connected to the grid. Then, the resultant sub-cycle impedance variations of the electrical grid were measured.

First, the effects of individual electronic devices on the sub-cycle impedance variations were obtained. As representative examples, Figs. 8 and 9 show the results of a group of 12 E27 LEDs (91 mA, 10.7 W) and a mobile phone charger (input AC 100–240V/50–60 Hz/65 mA, output DC 5V 350 mA), respectively. The figures illustrate the time variability of the magnitude and phase of the grid impedance within a mains cycle (20 ms) as a function of frequency, when these electronic devices are individually connected to the electrical grid.

As observed in the measurement results, high variations in both magnitude and phase of the grid impedance are generated by the electronic devices connected at that moment. The highest deviations are for high frequencies, above 4 MHz, where variations in magnitude are from a few Ohm to several hundreds of Ohm and changes in phase are from purely inductive to capacitive behavior.

These deviations correspond to two clearly differentiated states shown by the impedance of the electronic devices. When the diode-based rectifiers of these devices are in conducting state (ON), they show impedance values much smaller than the background grid impedance. As both impedances are in parallel, the equivalent impedance is very low and similar to the load impedance. On the contrary, when the diodes of the rectifier are in a non-conducting state (OFF), they show high impedance values, and the equivalent impedance is similar to the background grid impedance.

These results go in line with the impedance characterization of some electrical appliances found in [19], where a remarkable frequency selectivity of the impedance time variations is observed, with a clear two-state behavior during a cycle.

Second, the impact of several devices connected at the same time, in different points of the electrical grid of the laboratory, was measured (see Fig. 10). In this case, several laptop battery chargers, personal computers and fluorescent lamps were connected to the grid, working under normal uncontrolled operation. Therefore, the recording shows the time variability of the grid access impedance within a fundamental cycle under normal operation conditions, when the accumulative effects of the synchronous sub-cycle variations are present.

The results for the case of several electronic devices connected simultaneously to the grid are remarkable, as they provide the sharpest and highest changes, with several fast transitions from a few tens to more than 1700 Ohm within the mains cycle for the frequencies assigned to BB-PLC (see Fig. 10).

These abrupt changes in the impedance may have a relevant impact on the new BB-PLC technologies for several reasons. First, considering that the NB-PLC and BB-PLC transmission frames are from a few milliseconds to several tens of milliseconds [40], [41], [42], the data transmissions might significantly be affected by the changes within the mains cycle (four rapid and steep changes in a single mains period). Second, the sub-cycle impedance deviations between both states are present for the whole frequency band; still, they are particularly remarkable at the frequency range assigned to BB-PLC transmission technologies. The equalization algorithms that are being considered for BB-PLC technologies are not designed to consider such fast, huge and fast variations of the propagation channel. Consequently, the outcome of the equalization assessment in the receiver may be not valid for mitigating the effects of the impedance variations or even may cause detrimental effects on the quality of the communications. Therefore, new and advanced equalization algorithms that overcome the fast and steeped variations should be developed, tested, and incorporated into BB-PLC technologies.
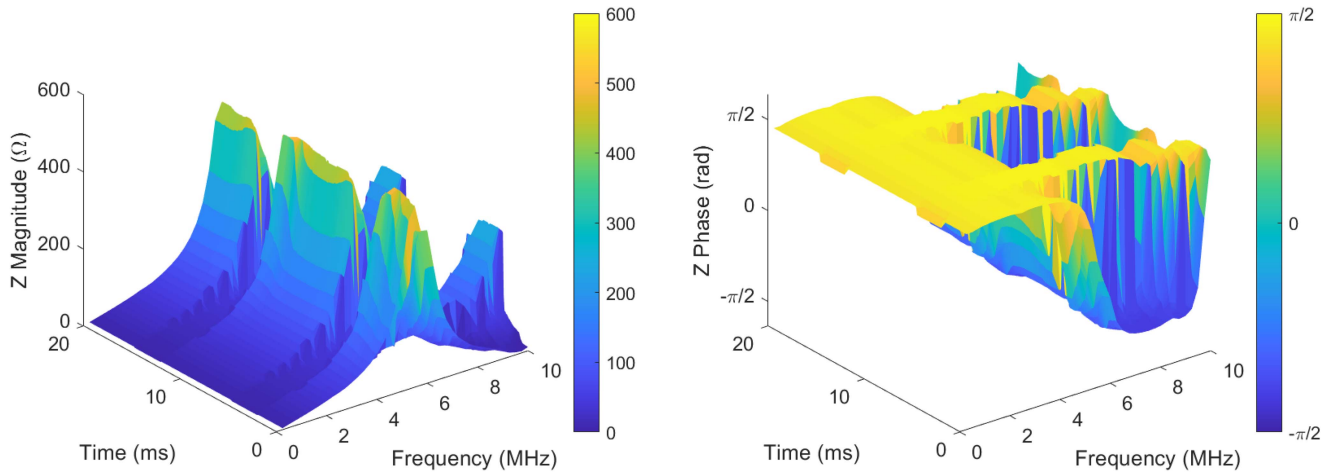
Fig. 8.   Sub-cycle impedance of the electrical grid when a group of LEDs is connected to the grid: (Left) magnitude, (right) phase.
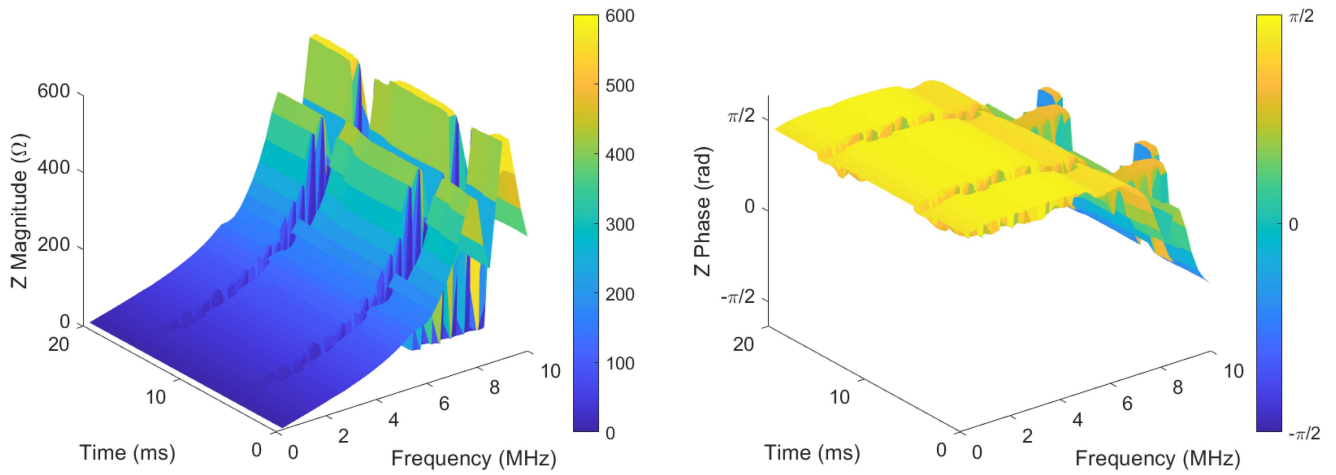

Fig. 9.   Sub-cycle impedance of the electrical grid when a mobile phone charger is connected to the grid: (Left) magnitude, (right) phase.
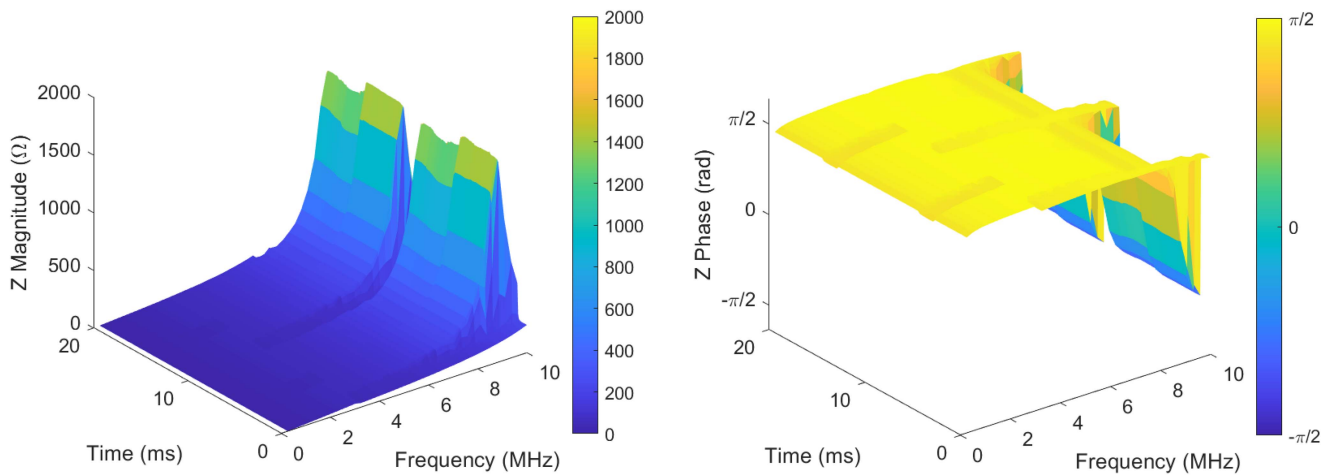

Fig. 10.   Sub-cycle impedance of the electrical grid when several electronic devices are connected to the grid: (Left) magnitude, (right) phase.

V. CONCLUSION

This paper proposes a measurement methodology and a specific setup based on laboratory equipment and additional circuitry in order to characterize the mean and sub-cycle impedance variations in the LV distribution grid. The system is valid for the frequency range assigned to NB-PLC (20 kHz to 500 kHz) and BB-PLC Mode 1 (2 MHz to 7 MHz) technologies. It is suitable for laboratory conditions, in-home networks, and field trials in the LV distribution grid, where a wide dynamic range and strong protection mechanisms against high-amplitude impulsive noises are required.

The accuracy of the measurement system was evaluated in a controlled and reproducible laboratory scenario by comparing the outputs to a precision impedance meter, which was used as a reference. The results of this analysis show a high degree of accuracy of amplitude and phase measurements for the entire frequency range under study.

Some representative measurements of the variations generated by electronic devices directly connected to the grid have been also developed in this work. These measurements aimed to evaluate the impedance variations induced by the electronic devices on the grid impedance. The results demonstrate that the grid impedance is highly time-varying within the mains cycle, both in amplitude and phase. The deviations are more remarkable for higher frequencies, which are assigned to BB-PLC technologies. Consequently, these transmission technologies can be particularly affected by these variations. Therefore, extensive field trials to examine the long-term and short-term variations of the grid impedance are required to gain knowledge on the propagation channel variations for BB-PLC technologies. In this context, the proposed measurement system is a novel and valuable tool for characterizing mean and sub-cycle impedance variations in the LV grid.

REFERENCES

[1] L. Lampe, A. M. Tonello, and T. G. Swart, "Power line communications," in *Principles, Standards and Applications from Multimedia to Smart Grid*, 2nd ed. Hoboken, NJ, USA: Wiley, 2016.

[2] G. López et al., "The role of power line communications in the smart grid revisited: Applications, challenges, and research initiatives," *IEEE Access*, vol. 7, pp. 117346–117368, 2019.

[3] N. Uribe-Pérez, L. Hernández, D. de la Vega, and I. Angulo, "State of the Art and trends review of smart metering in electricity grids," *Appl. Sci.*, vol. 6, no. 3, 2016, Art. no. 68.

[4] C. Cano, A. Pittolo, D. Malone, L. Lampe, A. M. Tonello, and A. G. Dabak, "State of the Art in power line communications: From the applications to the medium," *IEEE J. Sel. Areas Commun.*, vol. 34, no. 7, pp. 1935–1952, Jul. 2016.

[5] *Signalling on Low-Voltage Electrical Installations in the Frequency Range 3 kHz to 148.5 kHz. Part 1: General Requirements, Frequency Bands and Electromagnetic Disturbances*, CENELEC Standard - EN 50065-1, CENELEC, Brussels, Belgium, 2011.

[6] *Study Report on Electromagnetic Interference Between Electrical Equipment/Systems in the Frequency Range Below 150 kHz*, CENELEC Standard CLC/TR 50627, CENELEC SC 205A Mains Communicating Systems, CENELEC, Brussels, Belgium, 2015.

[7] S. Raponi, J. H. Fernandez, A. Omri, and G. Oligeri, "Long-term noise characterization of narrowband power line communications ${measurements, analysis and modeling}$," *IEEE Trans. Power Del.*, vol. 37, no. 1, pp. 365–373, Feb. 2022.

[8] D. Cooper and T. Jeans, "Narrowband, low data rate communications on the low-voltage mains in the CENELEC frequencies. I. Noise and attenuation," *IEEE Trans. Power Del.*, vol. 17, no. 3, pp. 718–723, Jul. 2002.

[9] *Investigation Results on Electromagnetic Interference in the Frequency Range Below 150 kHz*, CENELEC Standard CLC/TR 50669, CENELEC, Brussels, Belgium, Dec. 2017.

[10] A. Llano, D. de la Vega, I. Angulo, and L. Marron, "Impact of channel disturbances on current narrowband power line communications and lessons to be learnt for the future technologies," *IEEE Access*, vol. 7, pp. 83797–83811, 2019.

[11] G. Hallak, C. Nieß, and G. Bumiller, "Accurate low access impedance measurements with separated load impedance measurements on the power-line network," *IEEE Trans. Instrum. Meas.*, vol. 67, no. 10, pp. 2282–2293, Oct. 2018.

[12] J. Anatory, N. Theethayi, R. Thottappillil, M. M. Kissaka, and N. H. Mvungi, "The influence of load impedance, line length, and branches on underground cable power-line communications (PLC) systems," *IEEE Trans. Power Del.*, vol. 23, no. 1, pp. 180–187, Jan. 2008.

[13] I. Fernández, A. Arrinda, I. Angulo, D. de la Vega, N. Uribe-Pérez, and A. Llano, "Field trials for the empirical characterization of the low voltage grid access impedance from 35 kHz to 500 kHz," *IEEE Access*, vol. 7, pp. 85786–85795, 2019.

[14] C. Nieß, J.-P. Kitzig, and G. Bumiller, "Measurement system for time variable subcycle impedance on power lines," in *Proc. IEEE Int. Instrum. Meas. Technol. Conf.*, 2021, pp. 1–6.

[15] M. Antoniali, A. M. Tonello, and F. Versolatto, "A study on the optimal receiver impedance for SNR maximization in broadband PLC," *J. Elect. Comput. Eng.*, vol. 2013, pp. 1–11, 2013.

[16] S. Liu, B. Gou, H. Li, and R. Kavasseri, "Power-line communication channel characteristics under transient model," *IEEE Trans. Power Del.*, vol. 29, no. 4, pp. 1701–1708, Aug. 2014.

[17] I. Fernández, M. Alberro, J. Montalbán, A. Arrinda, I. Angulo, and D. de la Vega, "A new voltage probe with improved performance at the 10 kHz –500 kHz frequency range for field measurements in LV networks," *Measurement*, vol. 145, pp. 519–524, 2019.

[18] B. Wang and Z. Cao, "A review of impedance matching techniques in power line communications," *Electronics*, vol. 8, no. 9, 2019, Art. no. 1022.

[19] F. J. C. Corripio, J. A. C. Arrabal, L. D. del Rio, and J. T. E. Munoz, "Analysis of the cyclic short-term variation of indoor power line channels," *IEEE J. Sel. Areas Commun.*, vol. 24, no. 7, pp. 1327–1338, Jul. 2006.

[20] D. Chakravorty, J. Meyer, P. Schegner, S. Yanchenko, and M. Schocke, "Impact of modern electronic equipment on the assessment of network harmonic impedance," *IEEE Trans. Smart Grid*, vol. 8, no. 1, pp. 382–390, Jan. 2017.

[21] H. C. Ferreira, *Power Line Communications: Theory and Applications For Narrowband and Broadband Communications Over Power Lines*. Hoboken, NJ, USA: Wiley, 2010.

[22] J. González-Ramos, I. Angulo, I. Fernández, A. Arrinda, and D. de La Vega, "Characterization of the potential effects of EMC filters for power converters on narrowband power line communications," *Electronics*, vol. 10, no. 2, 2021, Art. no. 152.

[23] M. Antoniali and A. M. Tonello, "Measurement and characterization of load impedances in home power line Grids," *IEEE Trans. Instrum. Meas.*, vol. 63, no. 3, pp. 548–556, Mar. 2014.

[24] *Consideration of Reference Impedances and Public Supply Network Impedances for Use in Determining Disturbance Characteristics of Electrical Equipment Having a Rated Current ≤75 a Per Phase*, IEC/TR 60725:2012, IEC, Geneva, Switzerland, 2012.

[25] C. Unger, K. Krüger, M. Sonnenschein, and R. Zurowski, "Disturbances due to voltage distortion in the kHz range – experiences and mitigation measures," in *Proc. IEEE 18th Int. Conf. Exhib. Electricity Distrib.*, 2005, pp. 1–5.

[26] R. S. Singh, V. Ćuk, and S. Cobben, "Measurement-based distribution grid harmonic impedance models and their uncertainties," *Energies*, vol. 13, no. 16, Aug. 2020, Art. no. 4259.

[27] D. Serfontein, J. Rens, G. Botha, and J. Desmet, "Continuous event-based harmonic impedance assessment using online measurements," *IEEE Trans. Instrum. Meas.*, vol. 65, no. 10, pp. 2214–2220, Oct. 2016.

[28] A. Rygg and M. Molinas, "Real-time stability analysis of power electronic systems," in *Proc. IEEE 17th Workshop Control Model. Power Electron.*, 2016, pp. 1–7.

[29] J. Sun, "Impedance-based stability criterion for grid-connected inverters," *IEEE Trans. Power Electron.*, vol. 26, no. 11, pp. 3075–3078, Nov. 2011.

[30] S. Shah et al., "Large-signal impedance-based modeling and mitigation of resonance of converter-grid systems," *IEEE Trans. Sustain. Energy*, vol. 10, no. 3, pp. 1439–1449, Jul. 2019, doi: 10.1109/TSTE.2019.2903478.

[31] I. Fernández et al., "Comparison of measurement methods of LV grid access impedance in the frequency range assigned to Nb–PLC technologies," *Electronics*, vol. 8, no. 10, 2019, Art. no. 1155.

[32] G. Hallak and G. Bumiller, "Impedance measurement of electrical equipment loads on the power line network," in *Proc. IEEE Int. Symp. Power Line Commun. Appl.*, 2017, pp. 1–6.

[33] R. Stiegler, J. Meyer, P. Schegner, and D. Chakravorty, "Measurement of network harmonic impedance in presence of electronic equipment," in *Proc. IEEE Int. Workshop Appl. Meas. Power Syst.*, 2015, pp. 49–54.

[34] C. Szymczyk, C. Nieß, and G. Bumiller, "An on-line measurement approach for EMI filter characterization," in *Proc. IEEE Int. Symp. Power Line Commun. Appl.*, 2021, pp. 90–95.

[35] I. Elfeki, T. Doligez, I. Aouichak, J. Lebunetel, and Y. Raingeaud, "A new method for input installation impedance measurement," in *Proc. IEEE Int. Symp. Power Line Commun. Appl.*, 2018, pp. 1–6.

[36] T. Reinikka, T. Roinila, and J. Sun, "Measurement device for inverter output impedance considering the coupling over frequency," in *Proc. IEEE 21st Workshop Control Model. Power Electron.*, 2020, pp. 1–7.

[37] *Electrical Safety in Low Voltage Distribution Systems Up to 1000 V a.c. and 1500 V d.c. - Equipment for Testing, Measuring or Monitoring of Protective Measures — Part 3: Loop Impedance*, IEC 61557-3:2007, IEC, Geneva, Switzerland, 2007.

[38] *Electromagnetic Compatibility (EMC). Part 4-19: Testing and Measurement Techniques: Test for Immunity to Conducted, Differential Mode Disturbances and Signaling in the Frequency Range 2 kHz to 150 kHz at a.c. Power Ports*, IEC 61000-4-19:2015, IEC, Geneva, Switzerland, 2015.

[39] Keysight Tecnhologies, "E4990A impedance analyzer. Data sheet," Aug. 2022. [Online]. Available: https://www.keysight.com/en/pd-2405177-pn-E4990A

[40] *Specification For PoweRline Intelligent Metering Evolution v1.4*. Brussels, Belgium: PRIME Alliance, 2014.

[41] *IEEE Standard for Broadband Over Power Line Networks: Medium Access Control and Physical Layer Specifications*, ANSI/IEEE Standard 1901-2010, Piscataway, NJ, USA, 2010.

[42] *IEEE Standard for Medium Frequency (Less Than 12 MHz) Power Line Communications for Smart Grid Applications*, IEEE Standard 1901.1-2018, Piscataway, NJ, USA, May 2018.

Igor Fernández (Member, IEEE) received the M.Sc. and Ph.D. degrees in telecommunication engineering from the University of the Basque Country (UPV/EHU), Bilbao, Spain, in 2001 and 2011, respectively. He is currently an Assistant Professor with the Department of Communications Engineering, UPV/EHU. His research focuses on characterization of smart grids for power line communications.

Alexander Gallarreta (Graduate Student Member, IEEE) received the B.Sc. and M.Sc. degrees in telecommunications engineering in 2019 and 2021, respectively, from the University of the Basque Country (UPV/EHU), Bilbao, Spain, where he is currently working toward the Ph.D. degree in mobile network information and communication technologies. His research focuses on signal processing for the analysis of low-voltage grid emissions measurement methods.

Jon González-Ramos (Graduate Student Member, IEEE) received the B.Sc. and M.Sc. degrees in telecommunications engineering from the University of the Basque Country (UPV/EHU), Bilbao, Spain, in 2019 and 2021, respectively. He is currently working toward the Ph.D. degree the TSR Research Group. Since 2018, he has been part of the TSR Research Group. His research interests include the characterization of the electrical grid as a transmission medium for power line communications signals, and the analysis and development of communication technologies used in smart grids.

Paul Wright received the B.Sc. and Ph.D. degrees in electrical and electronic engineering from the University of Surrey, Surrey, U.K., in 1987 and 2002, respectively.

He spent three years as a Research Fellow with the University of Surrey, Guildford, U.K., where he was involved in the field of spacecraft sensors and attitude control. This was followed by three years with the Central Electricity Research Laboratory, where he was involved in advanced control systems. In 1992, he joined the National Physical Laboratory, Teddington, U.K., where he is currently a Principal Research Scientist specializing in AC measurements and waveform analysis. He has coordinated five EU collaborative research and development projects. He was the Coordinator of the EU project on 2–150-kHz grid measurement Supra EMI.

David de la Vega (Senior Member, IEEE) received the M.S. and Ph.D. degrees in telecommunication engineering in 1996 and 2008, respectively. Since 1998, he has been an Associate Professor with the Department of Communications Engineering, University of the Basque Country (UPV/EHU), Bilbao, Spain.

He has been the Head Researcher of competitive research projects funded by European, national and regional calls and by industry. The results of his work were published in 48 indexed papers, and part of them are included in reports of regulatory and standardization bodies. His research focuses on the signal propagation, mainly on the analysis of the effects of different types of interferences on the data transmission. In the area of Smart Grids, he researches on the characterization of the electrical grid as propagation medium for data transmission, and on the effects of noise and disturbances on the communications.

Itziar Angulo (Member, IEEE) received the M.S. and Ph.D. degrees in telecommunications engineering from the University of the Basque Country, Bilbao, Spain, in 2007 and 2013, respectively. Since 2005, she has been a part of the Radiocommunications and Signal Processing (TSR) Research Group, University of the Basque Country.

After five years of postdoctoral experience, she is currently an Associate Professor with the Department of Applied Mathematics, University of the Basque Country. She is currently involved in the characterization of the electrical grid as a communication channel for PLC, and the study of new data transmission techniques for smart metering, monitoring, and management of the future smart grids.

Amaia Arrinda (Senior Member, IEEE) received the M.Sc. degree in telecommunications engineering in 1993 and the Ph.D. degree in 2001.

Since 2017, she has been a Full Professor with the University of the Basque Country (UPV/EHU), Bilbao, Spain. She is currently with the Communications Engineering Department, University of the Basque Country and a Member of the TSR (Radiocommunications and Signal Processing) Research Group. She has been involved in many research projects. She is the co-author of many journal and conference papers. Her expertise is in the empirical analysis of propagation, radiated, and conducted noise and broadcasting, mainly based on lab and field measuring campaigns. During the last ten years, her research focuses on defining measurement systems and methodologies for both electromagnetic radiated emissions and conducted emissions characterization. Electromagnetic Field (EMF) assessment is necessary to estimate exposure level. Otherwise, the research on measuring conducted emissions has been applied in Smart grids to validate Power Line Communications (PLC).